

## Deconfinement in SU(2) Yang-Mills theory as a center vortex percolation transition

M. Engelhardt, K. Langfeld, H. Reinhardt, and O. Tennert  
*Institut für Theoretische Physik, Universität Tübingen, D-72076 Tübingen, Germany*  
 (Received 29 September 1999; published 8 February 2000)

By fixing lattice Yang-Mills configurations to the maximal center gauge and subsequently applying the technique of center projection, one can identify center vortices in these configurations. Recently, center vortices have been shown to determine the string tension between static quarks at finite temperatures (center dominance); also, they correctly reproduce the deconfining transition to a phase with vanishing string tension. After verifying center dominance also for the so-called spatial string tension, the present analysis focuses on the global topology of vortex networks. General arguments are given supporting the notion that the deconfinement transition in the center vortex picture takes the guise of a percolation transition. This transition is detected in Monte Carlo experiments by concentrating on various slices through the closed vortex surfaces; these slices, representing loops in lattice universes reduced by one dimension, clearly exhibit the expected transition from a percolating to a non-percolating, deconfined, phase. The latter phase contains a large proportion of vortex loops winding around the lattice in the Euclidean time direction. At the same time, an intuitive picture clarifying the persistence of the spatial string tension in the deconfined phase emerges.

PACS number(s): 11.15.Ha, 12.38.Aw

### I. INTRODUCTION

The description of hadronic matter in terms of confined quark and gluon constituents carrying a color quantum number has opened the prospect of a new, deconfined, phase of matter in which colored excitations can propagate over distances much larger than typical hadronic sizes. In the framework of pure Yang-Mills theory, the transition to this new phase is thought to occur as a function of temperature. While compelling evidence for the deconfining phase transition has been collected in lattice Monte Carlo simulations [1,2], it is necessary to concomitantly develop an intuitive picture for the deconfinement phenomenon in order to be able to treat scenarios as complex as heavy ion collisions; such collision experiments, planned at the BNL Relativistic Heavy Ion Collider (RHIC) and CERN Large Hadron Collider (LHC), are hoped to produce lumps of deconfined matter in the near future.

The question of the deconfinement transition cannot be separated from an underlying picture of the confinement mechanism itself. Conversely, any purported mechanism of confinement should also be able to incorporate deconfinement. The present paper concentrates on the center vortex picture of confinement in the case of SU(2) color. This mechanism, initially proposed in [3–5], generates an area law for the Wilson loop by invoking the presence of vortices in typical configurations entering the Yang-Mills functional integral. These vortices are closed two-dimensional surfaces in four-dimensional space-time or, equivalently, closed lines in the three dimensions making up, e.g., a time slice. They carry flux such that they contribute a factor corresponding to a nontrivial center element of the gauge group to any Wilson loop whenever they pierce its minimal area; in the case of SU(2) color to be treated below, that is a factor of  $-1$ . If the vortices are distributed in space-time sufficiently randomly, then samples of the Wilson loop of value  $+1$  (originating from loop areas pierced an even number of times by vortices) will strongly cancel against samples of the Wilson loop of

value  $-1$  (originating from loop areas pierced an odd number of times by vortices), generating an area law falloff. The simplest [SU(2)] model visualization which demonstrates this is the following: Consider a universe of volume  $L^4$ , and a two-dimensional slice through it of area  $L^2$ , containing a Wilson loop spanning an area  $A$ . Generic vortices will pierce the slice at points; assume  $N$  of these points to be randomly distributed on the slice. Then the probability of finding  $n$  such points inside the Wilson loop area is binomial,

$$P_N(n) = \binom{N}{n} \left(\frac{A}{L^2}\right)^n \left(1 - \frac{A}{L^2}\right)^{N-n}, \quad (1)$$

and the expectation value of the Wilson loop becomes

$$\langle W \rangle = \sum_{n=0}^N (-1)^n P_N(n) = \left(1 - \frac{2\rho A}{N}\right)^N \xrightarrow{N \rightarrow \infty} e^{-2\rho A} \quad (2)$$

where the planar density of the intersection points  $\rho = N/L^2$  is kept constant as  $N \rightarrow \infty$ . One thus obtains an area law with string tension  $\kappa = 2\rho$ . In a more realistic calculation, one would e.g. take into account interactions between the vortices [6]; the proportionality constant  $\kappa/\rho$  turns out to be close to 1.4 in zero temperature lattice measurements [7,8] (a survey of existing data follows further below).

The emphasis of the present work, however, lies not on the relatively short-range properties of the vortices such as their thickness, but on their long-range topology. This is where the argument presented above has more serious shortcomings. For one, it suggests that the expectation value of a Wilson loop might depend on the area with which one chooses to span the loop. However, as a result of the closed nature of the vortices, the choice of area is in fact immaterial, as it should be. In a more precise, area-independent, manner of speaking than adopted above, the value a Wilson loop takes in a given vortex configuration should be derived from the linking numbers of the vortices with the loop. Now, the

above model visualization demonstrating an area law implicitly makes a strong assumption about the long-range topology of vortex configurations: For the intersection points of vortices with a given plane to be distributed sufficiently randomly on the plane to generate confinement, typical vortices or vortex networks (note that vortices are not forbidden to self-intersect) must extend over the entire universe. Consider the converse, namely that there is an upper bound to the space-time extension of single vortices or vortex networks. Then an intersection point of a vortex with a plane always comes paired with another such point a finite distance away, due to the closed character of the vortices. This pairing in particular would preclude an area law for the Wilson loop, as can be seen more clearly with the help of another simple model.

Consider a universe as above, but with the additional information that intersection points of vortices with a two-dimensional slice come in pairs at most a distance  $d$  apart. Then the only pairs which can contribute a factor of  $-1$  to a planar Wilson loop are ones whose midpoints lie in a strip of width  $d$  centered on the trajectory of the loop. Denote by  $p$  the probability that a pair which satisfies this condition actually does contribute a factor of  $-1$ . This probability is an appropriate average over the distances of the midpoints of the pairs from the Wilson loop, their angular orientations, the distribution of separations between the points making up the pairs, and the local geometry of the Wilson loop up to the scale  $d$ . The probability  $p$ , however, does not depend on the macroscopic extension of the Wilson loop. A pair which is placed at random on a slice of the universe of area  $L^2$  has probability  $p \cdot A/L^2$  of contributing a factor of  $-1$  to a Wilson loop, where  $A$  is the area of the strip of width  $d$  centered on the Wilson loop trajectory. To leading order,  $A = Pd$ , where  $P$  is the perimeter of the Wilson loop; subleading corrections are induced by the local loop geometry. Now, placing  $N$  pairs on a slice of the universe of area  $L^2$  at random, the probability that  $n$  of them contribute a factor of  $-1$  to the Wilson loop is

$$P_{N_{pair}}(n) = \binom{N_{pair}}{n} \left( \frac{pPd}{L^2} \right)^n \left( 1 - \frac{pPd}{L^2} \right)^{N_{pair}-n} \quad (3)$$

and, consequently, the expectation value of the Wilson loop for large universes is

$$\langle W \rangle = \sum_{n=0}^{N_{pair}} (-1)^n P_{N_{pair}}(n) \xrightarrow{N_{pair} \rightarrow \infty} e^{-\rho Pd} \quad (4)$$

where  $\rho = 2N_{pair}/L^2$  is the planar density of points. One thus observes a perimeter law, negating confinement, if the space-time extension of vortices or vortex networks is bounded. They must thus extend over the entire universe, i.e. percolate, in order to realize confinement.

Conversely, therefore, a possible mechanism driving the deconfinement transition in the vortex picture is that vortices, in a sense to be made more precise below, cease to be of arbitrary length, i.e. cease to percolate, in the deconfined phase [8]. The main result of the present work is that this is

indeed the case, implying that the deconfinement transition can be characterized as a vortex percolation transition.

Before entering into the details, it should be noted that a description of the deconfinement transition in terms of percolation phenomena has also been advocated in frameworks based on Yang-Mills degrees of freedom other than vortices. For one, electric flux is expected to percolate in the *deconfined* phase, while it does not percolate in the confined phase. Note that this is the reverse, or dual, of the magnetic vortex picture. General arguments related to electric flux percolation were recently advanced in [9]; also, specific electric flux tube models support this picture [10].

On the other hand, in the dual superconductor picture of confinement, it has been observed that the confined phase is characterized by the presence of a magnetic monopole loop percolating throughout the (lattice) universe, whereas the monopole configurations are considerably more fragmented in the deconfined phase and cease to percolate [11]. To the authors' knowledge, however, this is mainly an empirical observation and there is no clear physical argument connecting the deconfinement transition and monopole loop percolation. Indeed, there has been speculation that the two phenomena may be disconnected [11]. This should be contrasted with the vortex language, which, as discussed at length above, has the advantage of providing a clear physical picture motivating an interrelation between vortex percolation and confinement.

## II. TOOLS AND SURVEY OF EXISTING DATA

Before vortex clustering properties can be investigated in detail, some technical prerequisites have to be met; foremost, one must have a manageable definition of vortices, i.e. an algorithm which allows one to localize and isolate them in Yang-Mills field configurations. After the initial proposal of the center vortex confinement mechanism, a first hint of the existence of vortex configurations was provided by the Copenhagen vacuum [12] based on the observation that a constant chromomagnetic field in Yang-Mills theory is unstable with respect to the formation of flux tube domains in three-dimensional space. Later it was observed that the chromomagnetic flux associated with these domains indeed is quantized according to the center of the gauge group [13]. However, the theory of these flux tubes quickly became too technically involved to allow e.g. the study of global properties of the flux tube networks, especially at finite temperatures. In parallel, efforts were undertaken to define and isolate vortices on a space-time lattice. One definition, proposed by Mack and co-workers [14] and developed further by Tomboulis [15], introduces a distinction between thin and thick vortices, only the latter remaining relevant in the continuum limit. The defining property of these thick vortices is the nontrivial center element factor they contribute to a large Wilson loop when they pierce its minimal area. This definition has the advantage of being gauge invariant; on the other hand, it does not allow one to easily localize vortices in the sense of associating a space-time trajectory with them.

A different line of reasoning has only recently been developed in a series of papers by Del Debbio *et al.* [7,16–18].

One chooses a gauge which as much as possible concentrates the information contained in the field configurations on particular collective degrees of freedom, in the present case, the vortices. If this concentration of information is successful (more about this question further below), one obtains a good approximation of the dynamics by neglecting the residual deviations away from the chosen collective degrees of freedom, i.e. by projecting onto them. This type of approach was pioneered by 't Hooft, who introduced the class of Abelian gauges and the subsequent Abelian projection in order to study Abelian monopole degrees of freedom [19]. In complete analogy, one can introduce maximal center gauges [7,16–18], in which one uses the gauge freedom to choose link variables on a space-time lattice as close as possible to center elements of the gauge group. Subsequently, one can perform center projection, i.e. replace the gauge-fixed link variables with the center elements nearest to them on the group.

Given such a lattice of center elements, i.e. in the case of SU(2) color, a lattice with links taking the values  $\pm 1$ , center vortices are defined as follows: Consider all plaquettes in the lattice. If the links bordering the plaquette multiply to  $-1$ , then a vortex pierces that plaquette. These are precisely the vortices needed for the center vortex mechanism of confinement. To see this, one merely needs to apply Stokes' theorem: Consider a Wilson loop  $W$ , made up of links  $l = \pm 1$ , and an area  $A$  it circumscribes, made up of plaquettes  $p = \pm 1$  (the value of a plaquette is given by the product of the bordering links). Then

$$W = \prod_{l \in W} l = \prod_{p \in A} p \quad (5)$$

(the same letter was used here to denote both space-time objects and the associated group elements). In other words, the Wilson loop receives a factor of  $-1$  from every vortex piercing the area. Furthermore, the product of all plaquettes making up a three-dimensional elementary cube in the lattice is 1, since this product contains every link making up the cube twice. This fact, which in physical terms is a manifestation of the Bianchi identity, implies that every such cube has an even number of vortices piercing its surfaces; consequently, any projection of the lattice down to three dimensions contains only closed vortex lines. Since any cut through a two-dimensional vortex surface in four dimensions is thus a closed line, the original surface is also closed. Note that if one defines the dual lattice as a lattice with the same spacing  $a$  as the original one, shifted with respect to the latter by the vector  $(a/2, a/2, a/2, a/2)$ , then vortices are made up of plaquettes on the dual lattice.

In the work presented here, the specific maximal center gauge called “direct maximal center gauge” (see e.g. [7]) was used. This gauge is reached by maximizing the quantity

$$\sum_l |\text{tr } U_l|^2, \quad (6)$$

where  $l$  labels all the links  $U_l$  on the lattice. Center projection then means replacing

$$U_l \rightarrow \text{sgn tr } U_l. \quad (7)$$

In practice, the question of whether the gauge fixing and projection procedure indeed successfully concentrates the relevant physical information on the collective degrees of freedom being projected on is difficult to settle *a priori*; most often, this is tested *a posteriori* by empirical means. Success furthermore depends on the specific physics, i.e. the observable, under consideration. One carries out two Monte Carlo experiments, using the full Yang-Mills action as a weight in both cases, and samples the observable in question, such as e.g. the Wilson loop, using either the full lattice configurations or the center projected ones. If the results agree, one refers to this state of affairs as “center dominance” for that particular observable. Center dominance for the Wilson loop is interpreted as evidence that the center gauge concentrates the physical information relevant for confinement on the vortex degrees of freedom, and that consequently center projection, i.e. projection onto the associated vortex configuration, constitutes a good approximation. Center dominance has been verified for the long-range part of the static quark potential at zero temperature [see [16–18] for the SU(2) theory and [7] for the SU(3) theory].

This recent verification of center dominance has sparked renewed interest in the vortex picture of confinement. In establishing the relevance of vortex degrees of freedom for confinement, it provides the necessary basis for any further investigation of vortex properties. An observation analogous to center dominance has been made in the framework of the gauge-invariant vortex definition advanced by Tomboulis [20]. There, one samples both the quantities  $W$  and  $\text{sgn}(W)$ ,  $W$  denoting the Wilson loop;  $\text{sgn}(W)$  is interpreted as containing only the center vortex contributions to  $W$ , whereas all other fluctuations of the gauge fields are neglected. One finds that the expectation value of  $\text{sgn}(W)$  alone already provides the full string tension; i.e., one finds a gauge-invariant type of center dominance [see [20] for the SU(2) theory and [21] for the SU(3) theory]. Subsequently, it has been noted that this type of center dominance without gauge fixing can in fact be understood in quite simple terms [22], and that furthermore the density of center vortices arising on center-projected lattices without gauge fixing does not exhibit the renormalization group scaling corresponding to a finite physical density [23].

In parallel, other vortex properties were investigated. There is evidence in the SU(2) theory that the vortices defined by center gauging and center projection indeed localize thick vortices as defined by their center element contributions to linked Wilson loops [17,18]. In both the gauge-fixed and unfixed frameworks, the absence of vortices was shown to imply the absence of confinement [17,18,24]. In zero temperature lattice calculations using the maximal center gauge, the planar density of intersection points of vortices with a given surface was shown to be a renormalization group invariant, physical quantity in the SU(2) theory; cf. [25] (note erratum in [8]) and also [7]. This planar density equals approximately  $3.6/\text{fm}^2$  if one fixes the scale by positing a string tension of  $(440 \text{ MeV})^2$ . Also the radial distribution function of these intersection points on a plane is renormalization

group invariant [6]. Furthermore, if one takes into account the thickness of center vortices, they are able to account for the ‘‘Casimir scaling’’ behavior of higher representation Wilson loops, a feature which hitherto was considered incompatible with the vortex confinement mechanism [26,27]. Also, the monopoles generated by the maximal Abelian gauge have been found to lie on the center vortices identified in a subsequent (indirect) maximal center gauge, forming monopole-antimonopole chains [18]. Recently, a modified  $SU(2)$  lattice ensemble was investigated in which all center vortices had been removed, with the result that chiral symmetry is restored and all configurations turn out to belong to the topologically trivial sector [28].

The purpose of the present analysis is to confront the center vortex picture of confinement with the finite temperature transition to a deconfined phase observed in Yang-Mills lattice experiments. Some previous work on vortex properties at finite temperatures has already been carried out, generalizing the zero-temperature results surveyed above. For one, the authors reported some preliminary work in [8]. There, center dominance for the string tension between static quarks was verified at finite temperatures, and the transition to the deconfined phase with a vanishing string tension observed at the correct temperature in the center-projected theory. A depletion in the density of vortex intersection points with a plane extending in the (Euclidean) time and one space direction occurs as one crosses into the deconfined phase. The vortices are to a certain extent polarized in the time direction. However, the polarization is not complete; an area spanned by a Polyakov loop correlator is still pierced by a finite density of vortices. Thus, more detailed correlations between these vortex intersection points must induce the deconfinement transition; this led the authors to first conjecture in [8] that the deconfinement transition in the center vortex picture may be connected to global properties of vortex networks such as their connectivity.

Very recently, a related investigation into the global topology of the two-dimensional vortex surfaces in four space-time dimensions was reported in [29], including the case of finite temperatures. This investigation focused on properties such as orientability and genus of the surfaces, in particular, changes in these characteristics as one crosses into the deconfined phase. In the present work, the global properties of vortex surfaces are considered from a slightly different vantage point, namely specifically with a view to testing the heuristic arguments given in the Introduction, connecting confinement with percolation properties. For this purpose, it will be necessary to consider in more detail different slices of vortex surfaces; details follow below.

### III. SPATIAL STRING TENSION

Before doing so, a certain gap in the existing literature on center vortices at finite temperatures should be addressed. As already mentioned above, the basis for the center vortex picture of confinement is the empirical observation of *center dominance* for the Wilson loop. Without first establishing center dominance for an observable under investigation, a more detailed discussion of the manner in which vortex dy-

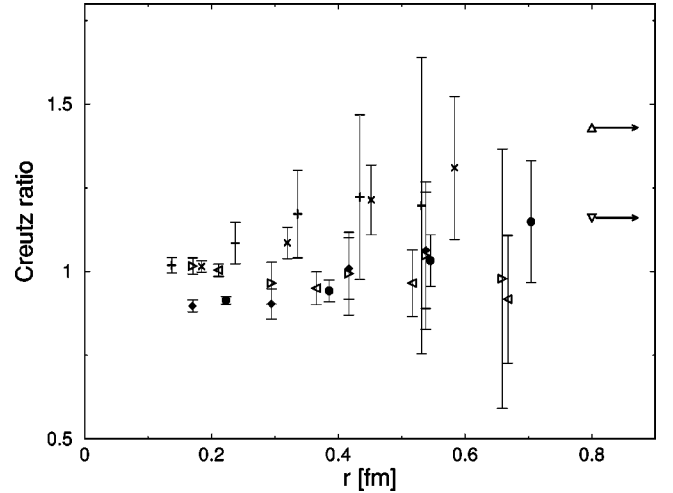


FIG. 1. Center-projected spatial Creutz ratios in units of the zero-temperature string tension,  $\kappa(T=0)a^2$ ;  $l \times l$  Creutz ratios are displayed at  $r = \sqrt{l(l-1)}a(\beta)$  on the horizontal axis. Measurements were taken on a  $12^3 \times N_t$  lattice. Shown are the temperatures  $T = 1.1T_C$  (open symbols; triangles pointing left correspond to  $\beta = 2.32$ ,  $N_t = 4$ , whereas triangles pointing right correspond to  $\beta = 2.4$ ,  $N_t = 5$ ),  $T = 1.4T_C$  (solid symbols; diamonds correspond to  $\beta = 2.4$ ,  $N_t = 4$ , whereas circles correspond to  $\beta = 2.3$ ,  $N_t = 3$ ), and  $T = 1.7T_C$  (crosses correspond to  $\beta = 2.48$ ,  $N_t = 4$ , whereas  $\times$ 's correspond to  $\beta = 2.37$ ,  $N_t = 3$ ). For comparison, the spatial string tension extracted from full Wilson loops, as interpolated from data reported by Bali *et al.* [30], is displayed: The triangle pointing downwards corresponds to  $T = 1.4T_C$ , whereas the triangle pointing upwards corresponds to  $T = 1.7T_C$ . The full spatial string tension at  $T = 1.1T_C$  is virtually indistinguishable from the zero-temperature value.

namics influences the observable runs the risk of being largely academic. Center dominance for the finite-temperature long-range heavy quark potential, via the corresponding Polyakov loop correlator, was verified in [8], as mentioned above; however, in what follows, also the behavior of the so-called spatial string tension, extracted from large spatial Wilson loops, will be under scrutiny. To provide the necessary basis for this, center dominance for large spatial Wilson loops should first be checked. For this purpose, the authors have carried out lattice measurements of spatial Creutz ratios, using center-projected configurations to evaluate the Wilson loops, for three temperatures.

Before presenting the results, a comment on the physical scales is in order. Throughout this paper, the zero-temperature string tension is taken to be  $\kappa = (440 \text{ MeV})^2$ , the lattice spacing  $a(\beta)$  at inverse coupling  $\beta = 2.3$  is determined by  $\kappa a^2 = 0.12$ , and one-loop scaling is used for the  $\beta$ -dependence of  $a$ . The deconfinement temperature is identified as  $T_C = 300 \text{ MeV}$ ; cf. [8]. It should be noted that these scales are fraught with considerable uncertainty, of the order of 10%, due to finite size effects. This was discussed in more detail in [8].

The values obtained for the center-projected spatial Creutz ratios are summarized in Fig. 1, where they are compared with the high-precision data for the full spatial string tension of Bali *et al.* [30]. Since the temperatures used here

and in [30] do not coincide, an interpolation of the data points given in [30] had to be carried out to arrive at the values depicted in Fig. 1.

Measurements were taken on a  $12^3 \times N_t$  lattice, and for each temperature, two values of the inverse coupling  $\beta$  were used. Note that there are two potential sources of scaling violations in Fig. 1. On the one hand, center projection may destroy the renormalization group scaling of the spatial string tension known to occur when using the full configurations [30]. This type of scaling violation would be a consequence, and thus a genuine indicator, of vortex physics. On the other hand, the manner in which the data is presented in Fig. 1 also engenders additional scaling violations to the extent to which Creutz ratios, which represent difference quotients with increment  $a(\beta)$ , still deviate from the derivatives they converge to as  $a \rightarrow 0$ . The authors have elected to accept this slight disadvantage, since the presentation of the data in Fig. 1 is on the other hand well adapted to aid in the discussion below. Now, comparing the data obtained for different  $\beta$  at one temperature in Fig. 1, scaling violations are evidently not significant as compared with the error bars. Namely, values of Creutz ratios for two different choices of  $\beta$  are well described by a universal curve, better in fact than the error bars would lead one to expect. However, in view of the size of the error bars, which is due to the moderate statistics available to the authors, the data do not give very stringent evidence of correct renormalization group scaling; they are perhaps best described as being compatible with such scaling.

Furthermore, the data seem to point towards a certain change in the dynamics generating the spatial string tension as the temperature is raised to values significantly above the deconfinement transition. At the temperature identified as  $T = 1.1T_C$ , the Creutz ratios are practically constant as a function of the Wilson loop size. This behavior of center-projected Wilson loops has been reported before in zero-temperature studies [17] and has been dubbed ‘‘precocious scaling.’’ Center projection truncates the short-range Coulomb behavior of full Wilson loops and one can read off the asymptotic string tension already from  $2 \times 2$  Creutz ratios.

By contrast, this behavior does not seem quite as pronounced at temperatures significantly above the deconfinement transition. Creutz ratios rise as a function of loop size; it should however be mentioned that this rise is much weaker than the usual Coulomb falloff one obtains when using the full Yang-Mills configurations to evaluate the Creutz ratios. As a result of this variation with loop size, the asymptotic value of the full spatial string tension extracted from the data in [30] is, in the case of  $T = 1.4T_C$ , only reached by the Creutz ratio corresponding to the largest Wilson loops investigated; at  $T = 1.7T_C$ , the asymptotic value is not quite reached even by the ratios derived from the most extended loops sampled, although it is within the error bars. While the error bars afflicting the Creutz ratios extracted from larger loops are sizable, the rise as a function of loop size does seem to be significant, especially as compared to the precocious scaling displayed at  $T = 1.1T_C$ . Also the difference between the values taken at  $T = 1.4T_C$  and  $T = 1.7T_C$  is com-

patible with the difference found for the full Wilson loops [30].

From the data depicted in Fig. 1, and in view of the above discussion, the authors estimate that, in the most unfavorable case admitted by the error bars, still 80% of the spatial string tension is furnished by center vortices in the temperature range above the deconfinement transition considered here. Thus, center vortices dominate the physics of the spatial string tension even in this temperature region.

## IV. VORTEX PERCOLATION

### A. Clustering of vortices

As already mentioned above, there exists even in the deconfined phase a substantial density of vortex intersection points on the area spanned by two Polyakov loops [8]. Thus, deconfinement must be due more specifically to a correlation between these intersection points, such that the distribution of points ceases to be sufficiently random to generate an area law. As motivated in the Introduction, a correlation conducive to deconfinement would occur if vortices only formed clusters smaller than some maximal size, i.e. if they ceased to percolate. This would make the points appear in pairs separated by less than the aforementioned maximal size, leading to a perimeter law for the Polyakov loop correlator. In order to test whether this type of mechanism is at work in connection with the Yang-Mills deconfinement transition, it is necessary to measure the extension of vortex clusters.

Vortices constitute closed two-dimensional surfaces in four space-time dimensions or, equivalently, one-dimensional loops if one projects down to three dimensions by taking a fixed time slice or a fixed space slice of the (lattice) universe. Note that the term space slice here is meant to denote the three-dimensional space-time one obtains by holding just one of the three space coordinates fixed. Which particular coordinate is fixed is immaterial in view of spatial rotational invariance. In the following, specifically the extension of vortex line clusters in either time or space slices will be investigated. In this way, the relevant information is exhibited more clearly than by considering the full two-dimensional vortex surfaces in four-dimensional space-time.

Given a center-projected lattice configuration, the corresponding vortices can be constructed on the dual lattice in the fashion already indicated in the Introduction. As a definite example, consider a fixed time slice. Then the vortices are described by lines made up of links on the dual lattice. Consider in particular a plaquette on the original lattice, lying e.g. in the  $z = z_0$  plane and extending from  $x_0$  to  $x_0 + a$  and from  $y_0$  to  $y_0 + a$ , where  $a$  denotes the lattice spacing. By definition, if the links making up this plaquette multiply to the center element  $-1$ , then a vortex pierces that plaquette. This means that a certain link on the dual lattice is part of a vortex, namely, the link connecting the dual lattice points  $(x_0 + a/2, y_0 + a/2, z_0 - a/2)$  and  $(x_0 + a/2, y_0 + a/2, z_0 + a/2)$ .

Having constructed the vortex configuration on the dual lattice, one can proceed to define the vortex clusters. One begins by scanning the dual lattice for a link which is part of a vortex. Starting from that link, one tests which adjacent

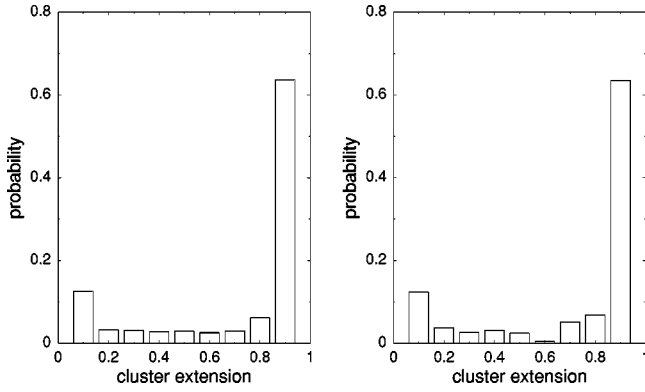


FIG. 2. Vortex material distributions in space slices of  $12^3 \times N_t$  lattice universes obtained as described in the text. Left:  $12^3 \times 8$  lattice at  $\beta=2.4$ , which is identified with  $T=0.7T_C$ . Right:  $12^3 \times 7$  lattice at  $\beta=2.4$ , which is identified with  $T=0.8T_C$ . The bins represent the percentage of vortex material organized into clusters of the corresponding extension. Extension is measured on the horizontal axis in units of the maximal extension possible on a space slice of the given lattice, namely  $\sqrt{2(12/2)^2 + (N_t/2)^2}$  lattice spacings.

links, i.e. links which share a dual lattice site with the first link, are also part of the vortex. This is repeated with all new members of the cluster until all links making up the cluster are found. In this way, it is possible to separate the different vortex clusters.

### B. Extension of vortex clusters

Given the vortex clusters, their extensions can be measured. Consider all pairs of links on a cluster and evaluate the space-time distance between each pair. The maximal such distance defines the extension of that cluster. In Figs. 2–5, histograms are displayed in which, for every cluster, the total number of links making up that cluster was added to the bin corresponding to the extension of the cluster.

The histograms were finally normalized such that the integral of the distributions gives unity. Constructed in this

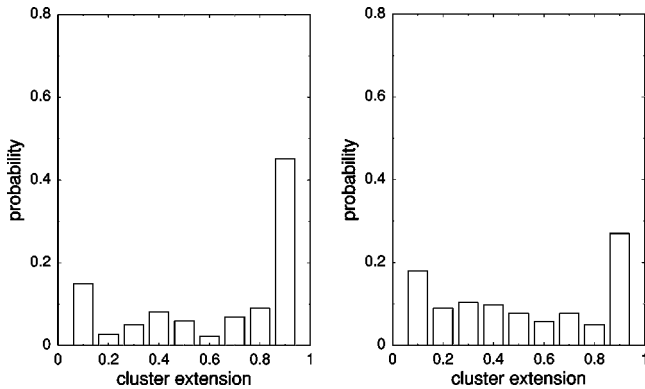


FIG. 3. Vortex material distributions as in Fig. 2, at different temperatures. Left:  $12^3 \times 6$  lattice at  $\beta=2.4$ , which is identified with  $T=0.9T_C$ . Right:  $12^3 \times 5$  lattice at  $\beta=2.4$ , which is identified with  $T=1.1T_C$ .

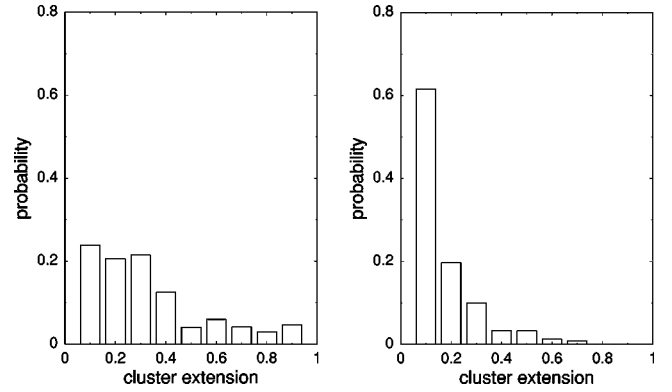


FIG. 4. Vortex material distributions as in Fig. 2, at different temperatures. Left:  $12^3 \times 4$  lattice at  $\beta=2.4$ , which is identified with  $T=1.4T_C$ . Right:  $12^3 \times 3$  lattice at  $\beta=2.4$ , which is identified with  $T=1.85T_C$ .

way, the histograms give a very transparent characterization of typical vortex configurations. The content of each bin represents the percentage of the total vortex length in the configurations, i.e. the available vortex material, which is organized into clusters of the corresponding extension. Accordingly, these distributions will be referred to as *vortex material distributions* in the following. In a percolating phase, the vortex material distribution is peaked at the largest extension possible on the lattice universe under consideration. Note that, due to the periodic boundary conditions, this maximal extension e.g. on a  $N_s \times N_s \times N_t$  space slice of the four-dimensional space-time lattice is  $\sqrt{(N_s/2)^2 + (N_s/2)^2 + (N_t/2)^2}$  lattice spacings. In a non-percolating phase, the vortex material distribution is peaked

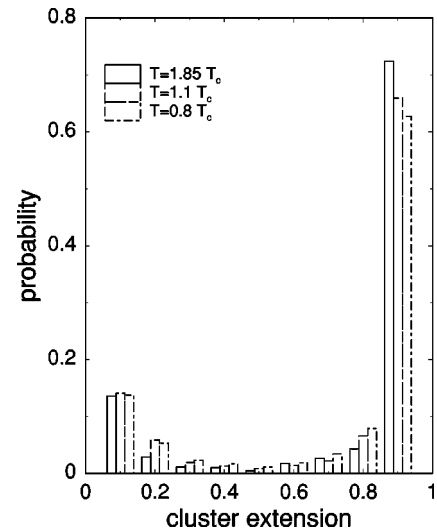


FIG. 5. Vortex material distributions analogous to Fig. 2, but taken from time slices of the  $12^3 \times N_t$  lattice universe, again at inverse coupling  $\beta=2.4$ . Bins corresponding to three different temperatures are shown simultaneously at each cluster extension: namely, the case  $N_t=3$ , which is identified with  $T=1.85T_C$ , the case  $N_t=5$ , which is identified with  $T=1.1T_C$ , and the case  $N_t=7$ , which is identified with  $T=0.8T_C$ .

at a finite extension independent of the size of the universe. Figures 2–4 pertain to space slices. Analogous results for time slices are summarized in Fig. 5.

In space slices of the lattice universe, one observes a transition from a percolating to a non-percolating phase at the Yang-Mills deconfinement temperature. Namely, in space slices, the vortex material distribution is strongly peaked at the maximal possible extension as long as the temperature remains below  $T_C$ ; when the temperature rises above  $T_C$ , however, the distribution becomes concentrated at short lengths. The behavior near the deconfinement temperature  $T_C$  displayed in Figs. 2–4 deserves more detailed discussion. While the contents of the bin of maximal extension fall sharply between  $T=0.8T_C$  and  $T=1.1T_C$ , a residual one-quarter of vortex material remains concentrated in loops of maximal extension at the temperature identified as  $T=1.1T_C$ . This is too large a proportion to let pass by without further consideration. The authors have repeated the measurement at  $T=1.1T_C$  on a larger,  $16^3 \times 3$  lattice, and did not find a depletion of the bin of maximal extension. On the other hand, one should be aware that there is a considerable uncertainty, of the order of 10%, in the overall physical scale in these lattice experiments, affecting in particular the identification of the deconfinement temperature  $T_C$  itself. These uncertainties were already mentioned in Sec. III and are discussed in detail in [8]. At the present level of accuracy,  $T=1.1T_C$  cannot be considered significantly separated from  $T_C$ ; the authors cannot state with confidence that the measurement formally identified with a temperature  $T=1.1T_C$  must unambiguously be associated with the deconfined phase. Note that also in standard string tension measurements via the Polyakov loop correlator, one does not attain a sharper signal of the deconfinement transition if one uses comparable lattices and statistics. Indeed, in [8], the authors still extracted a string tension of about 10% of the zero-temperature value at the temperature formally identified as  $T=1.1T_C$ .

In balance, the authors would argue that the percolation transition in space slices does occur together with the deconfining transition, both in view of the strong heuristic arguments connecting the two phenomena in the vortex picture and in view of the sharp change in the vortex material distributions between  $T=0.8T_C$  and  $T=1.1T_C$ . The latter sharp change suggests that the vortex material distributions can in practice be used as an alternative order parameter for the deconfinement transition. When the vortices rearrange at the transition temperature to form a non-percolating phase, intersection points of vortices with planes containing Polyakov loop correlators occur in pairs less than a maximal distance apart. This leads to a perimeter law for the Polyakov loop correlator, implying deconfinement.

Consider now by contrast the vortex material distributions obtained in time slices. According to Fig. 5, these distributions are strongly peaked at the maximal possible extension at all temperatures, even above the deconfinement transition. Thus, vortex line clusters in time slices always percolate; there is no marked change in their properties as the temperature crosses  $T_C$ .

Note that this entails no consequences for the behavior of the Polyakov loop correlator, since Polyakov loops do not lie within time slices. However, the persistence of vortex percolation into the deconfined phase when time slices are considered represents one way of understanding the persistence of a spatial string tension above  $T_C$ . Given percolation, it seems plausible that intersection points of vortices with spatial Wilson loops continue to occur sufficiently randomly to generate an area law. There is another, complementary, way of understanding the spatial string tension which will be discussed in detail in the concluding section.

Note furthermore that Figs. 2–5 taken together imply that the vortices, regarded as two-dimensional surfaces in four-dimensional space-time, percolate in both the confined and the deconfined phases; this was also observed in [29]. Only by considering a space slice does one filter out the percolation transition in the topology of the vortex configurations. It should be emphasized that the percolation of the two-dimensional vortex surfaces in four-dimensional space-time in the deconfined phase does not negate the heuristic picture of deconfinement put forward above. Given that vortex line clusters in space slices cease to percolate in the deconfined phase, intersection points of vortices with planes extending in one space and the time direction necessarily come in pairs less than a maximal distance apart, regardless of whether the different vortex line clusters do ultimately connect if one follows their world sheets into the additional spatial dimension. It is this pair correlation of the intersection points which induces the deconfinement transition.

### C. Winding vortices in the deconfined phase

In order to gain a more detailed picture of the deconfined regime, it is useful to carry out the following analysis. Consider again a space slice of the lattice universe, in which vortex line clusters are short in the deconfined regime. Consider in particular lattices of time extension  $N_t a$  with odd  $N_t$ , where  $a$  is the lattice spacing; in the following numerical experiment,  $N_t=3$ . On such a lattice, measure vortex material distributions akin to the ones described in the previous section, with one slight modification; namely, define the bins of the histograms not by cluster extension, but simply by the number of dual lattice links contained in the clusters. It turns out that, in the deconfined phase, specifically at  $T=1.85T_C$ , roughly 55% of the vortex material is concentrated in clusters made up of an odd number of links; cf. Fig. 6. On a lattice with  $N_t=3$ , these are necessarily vortex loops which wind around the lattice in (Euclidean) time direction by virtue of the periodic boundary conditions, where the loops containing an odd number of links larger than 3 exhibit residual transverse fluctuations in the spatial directions, as also visualized in Fig. 7 further below.

One thus obtains a quite specific characterization of the short vortices appearing in the deconfined regime. This phase can evidently be visualized largely in terms of short winding vortex loops with residual transverse fluctuations if one considers a space slice of the lattice universe; cf. Fig. 7. Note that this picture also explains the partial vortex polarization observed in density measurements [8].

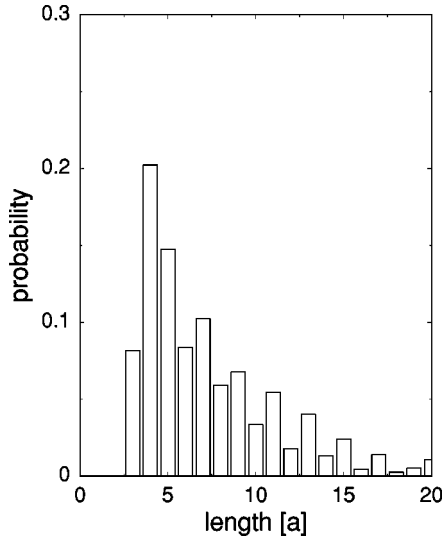


FIG. 6. Vortex material distributions in space slices of the lattice universe as a function of total vortex line length contained in the clusters. On the  $N_t=3$  lattice used, clusters with a length of an odd number of lattice spacings necessarily wind around the lattice in the Euclidean time direction. The inverse coupling in this measurement was again set to the value  $\beta=2.4$ , implying that this measurement is associated with a temperature of  $T=1.85T_C$ . There is a residual, but insignificant, proportion of vortex clusters containing more than 20 dual lattice links not displayed in the plot.

## V. DISCUSSION AND OUTLOOK

On the basis of the measurements shown in the preceding sections, a detailed description of the confined and deconfined phases of Yang-Mills theory in terms of center vortices emerges. The typical vortex configurations present in the two phases are visualized in Fig. 7. This picture allows an intuitive understanding of the phenomenon of confinement as well as the characteristics of the transition to the deconfined phase. In the confined phase, vortex line clusters in space slices of the lattice universe percolate. This allows intersection points of vortices with planes containing Polyakov loop correlators to occur sufficiently randomly to generate an area law. By contrast, in the deconfined phase, typical vortex configurations in space slices of the lattice universe are characterized by short vortex loops, to a large part winding in the (Euclidean) time direction. This causes intersection points of vortices with planes containing Polyakov loop correlators to occur in pairs less than a maximal distance apart, leading to a perimeter law. Simple analytical model arguments clarifying the emergence of this qualitative difference were presented in the Introduction. The deconfinement phase transition in the vortex picture can thus be understood as a transition from a percolating to a non-percolating phase.

It should be emphasized that the percolation properties of vortices focused on in the present work are more stringently related to confinement than the polarization properties reported in [8]. There is *a priori* no direct logical connection between the observed partial vortex polarization by itself and deconfinement. On the one hand, even in presence of a significant polarization, confinement would persist as long as the vortex loops retain an arbitrarily large length, namely by

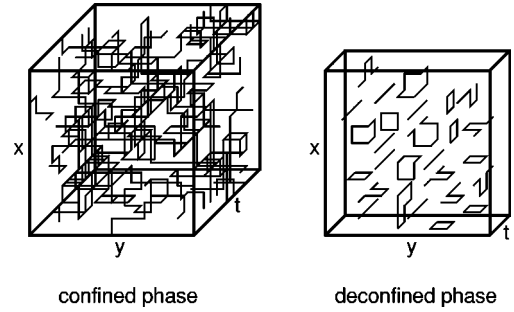


FIG. 7. Visualization of typical vortex configurations determining the long-range physics of the confined and deconfined phases of Yang-Mills theory. Note that this is not a depiction of particular configurations found in lattice experiments; rather, it is the authors' interpretation of the measurements shown in Figs. 2–6 in terms of typical configurations dominating the Yang-Mills functional integral in the confined and deconfined phases. Shown are space slices of the lattice universe obtained by holding the  $z$ -coordinate fixed. Slicing the two-dimensional vortex surfaces present in four space-time dimensions yields one-dimensional loop configurations such as depicted.

winding sufficiently often around the (Euclidean) time direction before closing. On the other hand, even in an ensemble with no polarization, deconfinement will occur if the vortices are organized into many small isolated clusters. Thus, vortex polarization should be viewed more as an accompanying effect than the direct cause of deconfinement. Of course, a correlation between the absence of percolation in space slices of the lattice universe and vortex polarization is not surprising. If fluctuations of vortex loops in the space directions are curtailed, e.g. due to a phase containing many short vortices winding in the time direction becoming favored (more about this below), then clearly the connectivity of vortex clusters in the space direction is reduced and they may cease to percolate. In this sense, polarization indirectly can facilitate deconfinement. However, the percolation concept is related much more directly and with much less ambiguity to the question of confinement. Ultimately, this is a consequence of a point already made in the Introduction in connection with the heuristic models discussed there. Since the Wilson loop should be independent of the choice of area which one may regard it to span, it is conceptually sounder not to consider densities occurring on such areas, but the global topology of the vortices such as their linking number with the Wilson loop. The likelihood of a particular linking number occurring is strongly influenced by the connectivity of the vortex networks. Correspondingly, there is a clear signal of the phase transition in the vortex material distributions displayed in Figs. 2–4; these quantities can be used as alternative order parameters for the transition. By contrast, the vortex densities seem to behave smoothly across the deconfinement phase transition [8].

Turning to the spatial string tension, there are two complementary ways to qualitatively account for its persistence in the deconfined phase of Yang-Mills theory. One was already mentioned in Sec. IV B. If one considers a time slice of the lattice universe, the associated vortex line configura-

tions display no marked change of their clustering properties across the deconfinement transition. Even in the deconfined phase, vortex loops in time slices percolate. In view of this, it seems plausible that intersection points of vortices with spatial Wilson loops continue to occur sufficiently randomly to generate an area law. It should be noted, however, that this percolation is qualitatively different from the one observed in the confined phase in that it only occurs in the three space dimensions, whereas the configurations are relatively weakly varying in the Euclidean time direction. In other words, in the deconfined phase, one finds a dimensionally reduced percolation phenomenon only visible either in the full four space-time dimensions or in time slices thereof.

On the other hand, if one considers a space slice of the lattice universe, the deconfined phase is characterized to a large part by short vortex loops winding in the time direction; cf. Fig. 7. However, in this topological setup, such short vortices can pierce the area spanned by a large spatial Wilson loop an odd number of times, even far from its perimeter. This should be contrasted with the picture one obtains for the Polyakov loop correlator. There, shortness of vortices implies that their intersection points with the plane containing the Polyakov loop correlator occur in pairs less than a maximal distance apart. This leads to a perimeter law behavior of the Polyakov loop correlator, i.e. deconfinement. For spatial Wilson loops, this mechanism is inoperative due to the different topological setting. On the contrary, in view of Fig. 7, if one assumes the locations of the various winding vortices to be uncorrelated, one obtains precisely the heuristic model of the Introduction, in which vortex intersection points are distributed at random on the plane containing the spatial Wilson loop, leading to an area law. Finite length vortex loops thus do not contradict the existence of a *spatial* string tension.

Of course, there is no reason to expect the locations of the winding vortices to be completely uncorrelated in the high-temperature Yang-Mills ensemble. In fact, comparing the values for the spatial string tension  $\kappa_s$  from [30] and the relevant density  $\rho_s$  of vortex intersection points on planes extending in two spatial directions [8], the ratio  $\kappa_s/\rho_s$  reaches values  $\kappa_s/\rho_s \approx 3$  at  $T \approx 2T_C$ . This should be contrasted with the value  $\kappa = 2\rho$  obtained in the model of random intersection points discussed in the Introduction. If one further takes into account that a sizable part of  $\rho_s$  is still furnished by non-winding vortex loops (cf. Fig. 6), then one should actually use the density  $\rho'_s < \rho_s$  corresponding to winding vortices only in the above consideration. This yields an even larger ratio  $\kappa_s/\rho'_s$ . Therefore, the winding vortices in the deconfined phase seem to be subject to sizable correlations.

Both of the above complementary mechanisms generating the spatial string tension in the deconfined phase are qualitatively distinct from the mechanism of confinement below  $T_C$ . In the space-slice picture, this is obvious; a new class of configurations, namely short vortex loops winding in the Euclidean time direction, induces the spatial string tension. However, as already indicated further above, also in the time-slice picture, the observed percolation is qualitatively different from the one in the confined phase in that it is

dimensionally reduced. This qualitatively different origin of the spatial string tension may provide a natural explanation for the novel behavior detected in Sec. III for spatial Creutz ratios at temperatures well inside the deconfined regime, namely, their rise as a function of the size of the Wilson loops from which they are extracted (as opposed to the precocious scaling observed at lower temperatures). However, the detailed connection between the abovementioned modified dynamics in the deconfined phase and the signal seen in the measurements of spatial Creutz ratios remains unclear.

While the relevant characteristics of the vortex configurations in the different regimes were described in detail in this work, the present understanding of the underlying dynamics in the vortex picture is still tenuous. There are, however, indications that the deconfining percolation transition can be understood in terms of simple entropy considerations. Increasing the temperature implies shortening the (Euclidean) time direction of the (lattice) universe. This means that the number of possible percolating vortex configurations decreases simply due to the reduction in space-time volume.<sup>1</sup> At the same time as the number of possible percolating vortex clusters is reduced, the number of available short vortex configurations is enhanced by the emergence of a new class of short vortices at finite temperature, namely the vortices winding in the time direction. In view of this, it seems plausible that a transition to a non-percolating phase is facilitated as the temperature is raised.

There are two pieces of evidence supporting this explanation, one of which was already given above. Namely, the deconfined phase indeed contains a large proportion of short winding vortices; cf. Fig. 6. More than half of the vortex material is transferred to the newly available class of short winding vortices in the deconfined phase. The second piece of evidence is related to the behavior of stiff random surfaces in four space-time dimensions; some of the authors plan to report on their Monte Carlo investigation of these objects in an upcoming publication [31]. The model assumes that the vortices are random surfaces associated with a certain action cost per unit area and a penalty for curvature of the vortex surface. By construction, evaluating the partition function of this model simply corresponds to counting the available vortex configurations under certain constraints imposed by the action; namely, the action cost per surface area effectively imposes a certain mean density of vortices, while the curvature penalty imposes an ultraviolet cutoff on the fluctuations of the vortex surfaces. Beyond this, no further dynamical

<sup>1</sup>For example, a vortex surface extending into two space directions has a greatly reduced freedom of transverse fluctuation into the time direction. Note that if one thinks of such a fluctuating, fuzzy thin vortex surface in terms of a thick envelope, this amounts to stating that the thick vortex extending into two space directions simply does not fit into the space-time manifold anymore. To a certain extent, the difference between these two (thin and thick vortex) pictures is semantic. To state that a thick vortex does not fit into the space-time manifold perpendicular to the time direction amounts to nothing but the statement that the number of possible configurations of this type has been reduced (to zero measure).

information enters. It turns out that already this simple model generates a percolation phase transition analogous to the one observed here for the center vortices of Yang-Mills theory. This suggests that the deconfining percolation transition of center-projected Yang-Mills theory can be understood in similarly simple terms, without any need for detailed assumptions about the form of the full center vortex effective action.

## ACKNOWLEDGMENTS

Discussions with F. Karsch and H. Satz are gratefully acknowledged. K.L. also acknowledges the friendly hospitality of the members of the KIAS, Korea, where a part of the numerical computations was carried out. M.E. is supported by Deutsche Forschungsgemeinschaft under DFG En 415/1-1.

- 
- [1] I. Montvay and G. Münster, *Quantum Fields on a Lattice* (Cambridge University Press, Cambridge, England, 1994).
- [2] H. J. Rothe, *Quantum Gauge Theories: An Introduction* (World Scientific, Singapore, 1997).
- [3] G. 't Hooft, Nucl. Phys. **B138**, 1 (1978).
- [4] Y. Aharonov, A. Casher, and S. Yankielowicz, Nucl. Phys. **B146**, 256 (1978).
- [5] J. M. Cornwall, Nucl. Phys. **B157**, 392 (1979).
- [6] M. Engelhardt, K. Langfeld, H. Reinhardt, and O. Tennert, Phys. Lett. B **431**, 141 (1998).
- [7] L. Del Debbio, M. Faber, J. Giedt, J. Greensite, and Š. Olejník, Phys. Rev. D **58**, 094501 (1998).
- [8] K. Langfeld, O. Tennert, M. Engelhardt, and H. Reinhardt, Phys. Lett. B **452**, 301 (1999).
- [9] H. Satz, Nucl. Phys. **A642**, 130 (1998).
- [10] A. Patel, Nucl. Phys. **B243**, 411 (1984); Phys. Lett. **139B**, 394 (1984).
- [11] V. G. Bornyakov, V. K. Mitrjushkin, and M. Müller-Preussker, Phys. Lett. B **284**, 99 (1992).
- [12] H. B. Nielsen and P. Olesen, Nucl. Phys. **B160**, 380 (1979); J. Ambjørn and P. Olesen, *ibid.* **B170** [FS1], 60 (1980); P. Olesen, *ibid.* **B200** [FS4], 381 (1982).
- [13] J. Ambjørn and P. Olesen, Nucl. Phys. **B170** [FS1], 265 (1980).
- [14] G. Mack and V. B. Petkova, Ann. Phys. (N.Y.) **123**, 442 (1979); **125**, 117 (1980); G. Mack, in *Recent developments in gauge theories*, edited by G. 't Hooft *et al.* (Plenum, New York, 1980); G. Mack, Phys. Rev. Lett. **45**, 1378 (1980); G. Mack and E. Pietarinen, Nucl. Phys. **B205** [FS5], 141 (1982).
- [15] E. T. Tomboulis, Phys. Rev. D **23**, 2371 (1981); Phys. Lett. B **303**, 103 (1993).
- [16] L. Del Debbio, M. Faber, J. Greensite, and Š. Olejník, Nucl. Phys. B (Proc. Suppl.) **53**, 141 (1997).
- [17] L. Del Debbio, M. Faber, J. Greensite, and Š. Olejník, Phys. Rev. D **55**, 2298 (1997).
- [18] L. Del Debbio, M. Faber, J. Greensite, and Š. Olejník, talk presented at the NATO Advanced Research Workshop on Theoretical Physics: New Developments in Quantum Field Theory, Zakopane, Poland, 1997, hep-lat/9708023.
- [19] G. 't Hooft, Nucl. Phys. **B190**, 455 (1981).
- [20] T. G. Kovács and E. T. Tomboulis, Phys. Rev. D **57**, 4054 (1998).
- [21] T. G. Kovács and E. T. Tomboulis, Phys. Lett. B **443**, 239 (1998).
- [22] J. Ambjørn and J. Greensite, J. High Energy Phys. **05**, 004 (1998); M. C. Ogilvie, Phys. Rev. D **59**, 074505 (1999).
- [23] M. Faber, J. Greensite, and Š. Olejník, J. High Energy Phys. **01**, 008 (1999).
- [24] T. G. Kovács and E. T. Tomboulis, hep-lat/9806030.
- [25] K. Langfeld, H. Reinhardt, and O. Tennert, Phys. Lett. B **419**, 317 (1998).
- [26] M. Faber, J. Greensite, and Š. Olejník, Phys. Rev. D **57**, 2603 (1998).
- [27] M. Faber, J. Greensite, and Š. Olejník, Acta Phys. Slov. **49**, 177 (1999).
- [28] P. de Forcrand and M. D'Elia, Phys. Rev. Lett. **82**, 4582 (1999).
- [29] R. Bertle, M. Faber, J. Greensite, and Š. Olejník, J. High Energy Phys. **03**, 019 (1999).
- [30] G. S. Bali, J. Fingberg, U. M. Heller, F. Karsch, and K. Schilling, Phys. Rev. Lett. **71**, 3059 (1993).
- [31] M. Engelhardt and H. Reinhardt, hep-lat/9912003.